Effects of α-crystallin gene knockout on zebrafish lens development

Mason Posner[1][*], Kelly L. Murray[1], Brandon Andrew[1], Stuart Brdicka[1], Alexis Roberts[1], Kirstan Franklin[1], Adil Hussen[1], Taylor Kaye[1], Emmaline Kepp[1], Mathew S. McDonald[1], Tyler Snodgrass[1], Keith Zientek[2] and Larry L. David[2]

[1]Department of Biology and Toxicology, Ashland University, Ashland, OH
[2]Department of Chemical Physiology & Biochemistry, Oregon Health and Science University

*Correspondence to:

Mason Posner
Ashland University, Department of Biology and Toxicology
401 College Avenue, Ashland, OH 44805
Phone: (419) 289-5691
email: mposner@ashland.edu

Competing Interests
Declarations of interest: none

Abstract

The α-crystallin small heat shock proteins contribute to the transparency and refractive properties of the vertebrate eye lens and prevent the protein aggregation that would otherwise produce lens cataracts, the leading cause of human blindness. There are conflicting data in the literature as to what role the α-crystallins may play in early lens development. In this study, we used CRISPR gene editing to produce zebrafish lines with null mutations for each of the three α-crystallin genes (*cryaa*, *cryaba* and *cryabb*). The absence of normal protein was confirmed by mass spectrometry, and lens phenotypes were assessed with differential interference contrast microscopy and histology. Loss of αA-crystallin produced a variety of lens defects with varying severity in larval lenses at 3 and 4 dpf but little substantial change in normal fiber cell denucleation. Loss of either αBa- or full-length αBb-crystallin produced no substantial lens defects. Mutation of each α-crystallin gene did not alter the mRNA levels of the remaining two, suggesting a lack of genetic compensation. These data confirm a developmental role for αA-crystallin in lens development, but the range of phenotype severity suggests that its loss simply increases the chance for defects and that the protein is not essential. Our finding that *cryaba* and *cryabb* mutants lack noticeable lens defects is congruent with insubstantial transcript levels in lens epithelial and fiber cells. Future experiments can explore the molecular consequences of *cryaa* mutation and causes of lens defects in this null mutant, as well as the roles of other genes in lens development and function.

Keywords: Lens, CRISPR, Crystallins, Cataract, Zebrafish,

1. Introduction

Alpha crystallins are small heat shock proteins that contribute to the high protein density that produces the refractive power of the vertebrate eye lens (Horwitz, 1992). Because of their ability to bind denaturing proteins and block aggregation, α-crystallins are thought to prevent lens cataracts, the leading cause of human blindness worldwide. Their expression in tissues outside the eye, especially the broadly expressed αB-crystallin, also suggests that they may play diverse physiological roles (Srinivasan et al., 1992). Numerous studies link αB-crystallin to the physiology and disease of muscular and nervous tissue (Bova et al., 1999).

Zebrafish have been a valuable model for investigating lens crystallin function. Zebrafish and human lenses are made of similar proteins, and the mechanisms underlying their development are conserved (Greiling et al., 2010; Posner et al., 2008). The production of large numbers of transparent embryos and the ease with which zebrafish can be genetically manipulated make them a good tool for examining crystallin function. The presence of two αB-crystallin paralog genes in zebrafish provides an opportunity to dissect the roles of this multifunctional single mammalian protein (Smith et al., 2006). The accessibility of early-stage embryos and fast development times make zebrafish ideal for studying the roles of α-crystallins in early lens development. These studies in zebrafish are more convenient and less costly than in mammalian systems such as mice.

Various genetic knockout and translation blocking techniques have been used to investigate the impacts of α-crystallin loss on zebrafish lens development. These experiments showed that loss of any of the three α-crystallin genes produced lens defects in 3- and 4-day-old fish (Mishra et al., 2018; Zou et al., 2015). This result differed from work in mice, which showed that while the loss of αA-crystallin led to reduced lens size and early cataract development, the loss of αB-crystallin did not produce a lens phenotype, although heart defects were found (Brady et al., 2001, 1997). Furthermore, our recent analysis of zebrafish gene expression at single-cell resolution indicated that neither of the two αB-crystallin genes were expressed in the lens at substantial levels through five days of development (Farnsworth et al., 2021). Therefore, there seem to be conflicting reports on what role, if any, αB-crystallins play in early lens development.

In the present study, we examined the larval lens in newly generated knockout lines for all three zebrafish α-crystallin genes. The resulting data address open questions about what effect, if any, the loss of either αB-crystallin protein will have on lens development. We also provide a more detailed analysis of lens phenotypes after αA-crystallin loss and compare several approaches for producing gene knockouts using CRISPR editing. This data analysis can provide a set of best practices for future studies of lens gene function.

2. Materials and Methods

2.1. Fish maintenance and treatment

All experiments performed with zebrafish in this study were approved by Ashland University's Animal Use and Care Committee (approval #MP 2019-1) and the reporting in the manuscript follows the recommendations in the ARRIVE guidelines (Kilkenny et al., 2010). Methods of anesthesia and euthanasia, as described below, were consistent with the *Guidelines for Use of Zebrafish in the NIH Intramural Research Program* and were in accordance with the AVMA guidelines. ZDR strain zebrafish were maintained on a recirculating aquarium system at approximately 28°C with a 14:10 light and dark cycle with daily water changes. Juveniles and adults were fed twice each day with a combination of dry flake food and live *Artemia* cultures. Adults were bred in separate false bottom tanks to collect fertilized eggs, which were incubated in petri dishes with system water at 28°C. The resulting larvae that were to be raised to adulthood were fed a liquid slurry of ground zooplankton and green algae until large enough to eat flake food and *Artemia*.

2.2. Guide RNA design, production and injection

Target regions for the guide RNA (gRNA) used in single and double injections to produce null lines were identified using the CRISPR design tool in the *Benchling* digital notebook system (www.benchling.com). The target regions for the four-gRNA mix used to produce *cryaa* crispants were identified by Wu et al. 2018 (Wu et al., 2018). Sequences for all gRNA primers are shown in Supplementary Table S1. Guide RNAs were produced using a PCR-based plasmid-free approach that annealed and elongated a universal scaffold primer with one, two or four additional primers containing the sequence of the target region. Equimolar amounts of universal scaffold primer and target region primers were used with Q5 DNA polymerase (NEB). Cycling parameters included a touchdown PCR protocol: initial 94°C denaturation for 5 min; cycle parameters: 94°C for 20 sec, 65° for 20 sec, 68°C for 15 sec (13 additional cycles with extension temperature reduced 0.5°C per cycle); 30 additional cycles of 94°C for 20 sec, 58°C for 20 sec, 68°C for 15 sec; final extension 68°C for 5 minutes. The resulting PCR product was purified with the Monarch PCR and DNA Cleanup Kit (NEB) with elution in 20 microliters nuclease-free water. Up to 1000 ng of purified PCR product was used with the HighScribe T7 kit (NEB) and incubated overnight at 37°C, and the reaction was purified with the Monarch RNA Cleanup Kit (500 micrograms) with elution in 50 μl nuclease-free water (NEB). The quality of the gRNA prep was confirmed by agarose gel electrophoresis and quantified using a NanoDrop One (Thermo Fisher).

Each injection mix contained 250 ng/μl total of the purified gRNAs and 500 ng/μl of recombinant Cas9 protein (PNA Bio) with 0.2% phenol red in nuclease-free water. One nanoliter of mix was microinjected with a single 20 millisecond pulse into the cytoplasm of each zebrafish zygote using a Harvard Apparatus PL-90 picoinjector (Holliston, MA).

2.3. Identification of null lines

Embryos injected with single or double gRNAs were genotyped after at least two months of age. Fish were anesthetized in 0.016% tricaine methane sulfonate (MS-222) resuspended in trisma base, and the posterior edge of the fin was removed with scissors. Fish were kept separated for recovery and during genotyping. Genomic DNA was collected from each fin clip using the Monarch Genomic DNA

125 Purification kit (New England Biolabs) and amplified using OneTaq 2X Master Mix (NEB) with PCR
126 primers that flanked the gRNA-targeted region. The recommended PCR protocol was followed, with
127 appropriate annealing temperatures determined experimentally. All primers and annealing
128 temperatures are shown in Supplementary Table S1. Amplified genomic DNA targeted with one gRNA
129 was sequenced to determine whether more than one sequence was apparent beginning at the target
130 area. Mutated genomic regions targeted with two gRNAs could be identified directly by the size of the
131 resulting PCR product and then sequenced to confirm the resulting allele.
132
133 Fish resulting from injected zygotes (founder fish: F0) determined through fin clipping to contain
134 mutant alleles were outcrossed to wild-type fish. Ten resulting embryos were combined and
135 homogenized to purify genomic DNA, and the targeted gene region was amplified to determine if the
136 parent founder fish had passed on mutant alleles to offspring. If offspring were found to be
137 heterozygous for a gene mutation, larvae were raised another two months for fin clipping. For single
138 gRNA-injected fish, sequencing of the heterozygotes was performed to determine if the resulting
139 mutation would cause a frame shift and early stop codon. Multiple heterozygotes with the same
140 identified frameshift mutation were incrossed to produce null individuals that were then used to
141 produce null lines. For double gRNA-injected embryos, sequencing was used to identify heterozygotes
142 with the same deletion, which were then incrossed to generate a null line.
143
144 *2.4. Proteomic assessment of knockout fish*
145 A detailed protocol outlining the sample preparation of zebrafish lenses to detect the presence of α-
146 crystallins was previously published (Posner et al., 2017). Briefly, 50 μg portions of protein derived
147 from either one or two dissected lenses were digested overnight with trypsin in the presence of
148 ProteaseMax™ detergent as recommended by the manufacturer (ProMega, Madison, WI, USA). One
149 microgram of each tryptic digest was then injected at 10 μl/min onto a Symmetry C18 peptide trap
150 (Waters Corporation, Milford, MA, USA) for 0-5 min using 98% water, 2% acetonitrile (ACN), and 0.1%
151 formic acid mobile phase and then switched onto a 75 μm x 250 mm NanoAcquity BEH 130 C18 column
152 (Waters Corporation) using mobile phases water (A) and ACN (B), each containing 0.1% formic acid.
153 Peptides were separated using 7.5-30% ACN over 5-35 min, 30-98% from 35-36 min, 98% ACN from 36-
154 41 min, 98-2% ACN from 41-42 min, and 2% ACN from 41-60 min at a 300 nL/min flow rate. Eluent was
155 analyzed using a Q-Exactive HF mass spectrometer using electrospray ionization with a Nano Flex Ion
156 Spray Source fitted with a 20 μm stainless steel nanobore emitter spray tip and 1.0 kV source voltage
157 (Thermo Fisher Scientific, San Jose, CA, USA). Xcalibur version 4.0 was used to control the system. Prior
158 to the targeted parallel reaction monitoring data collection, a digest from an adult 12-month old wild-
159 type lens was analyzed by data-dependent acquisition (DDA) to produce a zebrafish spectral library to
160 design a targeted parallel reaction monitoring (PRM) method to measure the abundance of αA, αBa,
161 and αBb-crystallins in wild-type and mutant fish. Precursor mass spectra were acquired over m/z 375
162 to 1,400 m/z at 120,000 resolution, automatic gain control (AGC) target 3 x 10^6, maximum ion time
163 (MIT) of 50 ms, profile mode, and lock mass correction using m/z = 445.12002 and 391.28429
164 polysiloxane ions. MS2 scans were acquired from 200-2000 m/z, intensity threshold of 5 x 10^4,
165 automatic gain control (AGC) 1 x 10^5, maximum ion time (MIT) 100 ms, 30,000 resolution, profile
166 mode, normalized collision energy (NCE) 30, isolation window of 1.2 m/z, loop count 10, and exclusion
167 of +1 and unassigned charges. MS2 results were searched using Sequest within Protein Discoverer 1.4
168 (Thermo Fisher Scientific) using a tryptic search, 10 ppm precursor mass tolerance, 0.1 Da fragment ion

169 tolerance, dynamic modification for oxidation of methionine, and a static modification of cysteines for
170 carbamidomethyl alkylation. A uniprot filtered proteome 000000437 zebrafish protein database
171 containing 43,607 entries downloaded on 5/17/2022 was used. Control of peptide false discovery used
172 a reversed sequence strategy and Percolator software to calculate q scores. Skyline (v.22.2.0.255)
173 (Pino et al., 2020) was then used to create a Biblio Spec spectral library containing 564 peptide entries
174 using a cutoff score of 0.95. These peptides were associated with the above uniprot zebrafish database
175 to match to 434 proteins and peptides matching αA-, αBa-, and αBb-crystallins were added to the
176 target list. The raw file used to create this spectral library was then imported into Skyline and 3
177 peptides from each protein were selected that had both strong precursor intensities and complete
178 fragment ion series. This precursor list was exported to create a PRM method within the instrument
179 control software with identical chromatographic conditions as used in the DDA run. Precursor scans
180 from 400-1000 m/z at 120,000 resolution were used with AGC 1 x 10^6, MIT 200 ms, profile mode, and
181 mass lock mass correction as above. PRM scans used a loop count of 10, 15,000 resolution, AGC target
182 2 x 10^5, MIT 100 ms, NCE 26, and isolation window 2.0 m/z. The results were processed using Skyline
183 Software and were deposited into the Panorama Public database with the unique identifier XXXX
184 (*accession number pending*).
185
186 *2.5. Phenotype assessment*
187 Embryos produced by incrossing the null lines were treated in 0.2 mM PTU in system water between 6
188 and 20 hours post-fertilization to maintain transparency. The gross anatomy of each larva was imaged
189 at 45 total magnification on a dissecting microscope, while one of their lenses was imaged at 200X
190 total magnification using differential interference microscopy on an Olympus IX71 microscope. Images
191 were taken with SPOT cameras and were cropped and oriented using ImageJ (NIH). The statistical
192 significance in differences in proportions of defect types between samples was calculated using the "N-
193 1" Chi-squared test (*https://www.medcalc.org/calc/comparison_of_proportions.php)* Lens diameters
194 were measured in ImageJ with a line spanning the equator of the lens, which differs from the anterior-
195 posterior dimension (Wang et al., 2020). Body lengths were measured from the tip of the snout to the
196 end of the axial skeleton. Any statistically significant differences in measurements between genotypes
197 were calculated using the *anova* and *Tukey HSD* functions in R (R. C. Team, 2020) within RStudio (Rs.
198 Team, 2020).
199
200 Larvae were anesthetized and then transferred to 4% paraformaldehyde with 5% sucrose for storage at
201 4°C until cryosectioning and DAPI staining to observe the presence of lens cell nuclei. The sectioning
202 procedure has been previously reported (Posner et al., 2013). The resulting slides with 10 micron lens
203 sections were mounted using Vectashield Antifade Mounting Medium with DAPI (Vector Laboratories)
204 and imaged on an Olympus IX71 microscope. DAPI intensity across the diameter of the lens was
205 measured using the Concentric Circles plugin for ImageJ. An oval was drawn matching the lens shape,
206 and 10 concentric circles were used to quantify the average pixel intensity along the perimeter of each
207 circle. Any statistically significant differences in average pixel intensity between genotypes at each
208 circle were calculated with a Mann–Whitney U test in R. All scripts and data used for this and other
209 non-mass spectrometric analyses in this study can be found in this repository on GitHub:
210 github.com/masonfromohio/alpha-crystallin-CRISPR-Rscripts. All lens images used in these analyses
211 are available on Dryad.org (submission pending).
212

213 *2.6. Quantitative PCR analysis of alpha crystallin expression*
214 The qPCR methods were designed to meet MIQE guidelines (Bustin et al., 2009) and followed methods
215 previously described (Posner et al., 2017). Larvae were collected at 7 dpf and stored in RNAlater
216 (Thermo) at 4°C for up to one month until used for purification of total RNA with the Monarch Total
217 RNA Miniprep Kit (NEB). Five larvae were pooled for each RNA purification and homogenized in
218 DNA/RNA protection buffer with a glass homogenizer prior to proteinase K digestion, following the kit
219 protocol. DNase treatment was performed in an RNA purification column, with a final elution in 50 μl
220 of nuclease-free water. The concentration of collected RNA was measured in a Nanodrop One (Thermo
221 Fisher). The ProtoScript II First Strand cDNA Synthesis Kit (NEB) was used with 600 ng of total RNA from
222 each sample with the d(T)23 VN primer using the standard protocol in a total volume of 20 μl, and -RT
223 controls were included.
224
225 Luna Universal qPCR Master Mix (NEB) was used to amplify 1.5 μl of each cDNA sample in a 20 μl total
226 reaction using the manufacturer's standard protocol on an Applied Biosystems StepOne Real-Time PCR
227 System (Thermo). Three technical replicates were used for each cDNA sample, while two technical
228 replicates were used with all -RT and nontemplate controls (water). Two endogenous control primer
229 sets were included (*rpl13a* and *ef1a*). All primer sequences and previously calculated efficiencies are
230 shown in Table 2 of Posner et al. (2017). Reactions included primers at a final concentration of 250 nm
231 with the following parameters: hold at 95°C for 1 min; 40 cycles of 95°C for 15 s and 60°C for 30 s; fast
232 ramp setting. Melt curve analysis was used to confirm that single products were produced, and
233 amplification products had previously been sequenced to confirm their expected identity (Posner et al.,
234 2017). Analysis of the resulting Cq values was identical to the process previously reported (Posner et
235 al., 2017).

6

3. Results

3.1. Disruption of cryaa produced several types of lens defects that ranged in severity

We used two approaches to mutate the zebrafish *cryaa* gene to prevent the production of αA-crystallin protein. First, we injected a single guide RNA (gRNA) to produce frame shift mutations and an early stop codon (Fig. 1A). This approach successfully produced a 5 base pair deletion and early stop codon after the leucine residue at position 27 (Fig. 1B). Mass spectrometry confirmed that this mutant prevented the production of any measurable αA-crystallin protein, as shown by the absence of αA-crystallin peptide 52-65 in the *cryaa -/-* lens (Fig. 1C, right). Two additional αA-crystallin peptides that were monitored were also missing in *cryaa -/-* lenses (Supplementary Fig. S1). Differential interference contrast (DIC) microscopy of anesthetized and PTU-treated larvae at 3 days postfertilization (dpf) showed that *cryaa* homozygous null fish (cryaa$^{-/-}$) had lens irregularities. These phenotypes included a central roughness and disorganization of central fiber cells compared to wild-type controls (Fig. 1 D-F). Because this original *cryaa* null line stopped breeding, we produced a second null line by using two gRNAs to produce an 863 bp deletion that removed a portion of the *cryaa* promoter and start codon region (Fig. 2A). This approach made it simpler to identify mutants by PCR (Fig. 2B) and reduced the potential for genetic compensation due to mutant mRNA degradation, as no truncated mRNA would be produced (El-Brolosy et al., 2019). The resulting *cryaa* null line bred well, lacked αA-crystallin peptides (Supplementary Fig. S1), and all further data presented are from these fish.

A substantial proportion of *cryaa* null larvae had lenses that appeared similar to those of wild-type fish (Fig. 2C). Others showed phenotypes that we classified into five categories. Some lenses had central roughness that appeared as many small darker spots in the region of the primary fiber cells (Fig. 2D). Some lenses contained elongated roughened areas that appeared to trace the edges of peripheral fiber cell boundaries (Fig. 2 D and E, black arrows). We also found lenses with a disorganization of central fiber cells (Fig. 2 E and F). These lenses did not show regular circular rings of central fiber cells. Some lenses showed more severe boundaries between fiber cells, possibly at the interface between the lens nucleus and cortex (Fig. 2G, black arrows), and some lenses exhibited large pitting (Fig. 2H).

3.2. Frame shift mutations of the two paralogs for zebrafish αB-crystallin genes did not produce significant overall lens defects

Single gRNAs were designed to target exon 1 in both the *cryaba* and *cryabb* genes (Fig. 3). Injected embryos were raised, and those with mutations leading to frameshifts and early stop codons were identified. A single basepair deletion in *cryaba* led to an altered amino acid sequence after residue 14 and a stop codon at residue 65 (Fig. 3B). Mass spectrometry indicated that lenses from *cryaba* mutant adults expressed no detectable αBa-crystallin, as evidenced by missing tryptic peptide 80-89 in the mutant lens (Fig. 3C, right). An 8 bp deletion in *cryabb* produced altered amino acids after residue 9 and a stop codon at residue 26 (Fig. 3D & E). Digests of adult *cryabb* homozygous mutant fish lenses had undetectable levels of peptide 12-20 (Fig. 3F, right). However, of the three peptides monitored in *cryabb* adult mutant lenses, the most C-terminal peptide (residues 82-92) was still detected (Supplementary Fig. S1). The *cryabb* mutant has a start codon in frame that could direct production of a partial peptide including residues 59 through 165, which is consistent with our mass spectrometry data.

7

279

280 The prevalence of lens defects in larvae generated by our *cryaa*, *cryaba* and *cryabb* mutant lines was

281 quantified at 3 and 4 dpf to assess the impacts of loss of each α-crystallin on lens development (Fig. 4).

282 Lens defects were statistically significantly increased in mutant *cryaa* larvae at both 3 and 4 dpf and in

283 *cryaa* crispant larvae at 4 dpf compared to wild-type larvae. There was no significant increase in overall

284 lens defects in the *cryaba* or *cryabb* mutant larvae. The appearance of central roughness was

285 characteristic of our *cryaa* null larvae and not significant in any other sample. Peripheral fiber cell

286 defects and severe fiber cell boundaries were significantly increased at some of our *cryaa* null and

287 crispant timepoints. While lower in proportion, these fiber cell defects were significantly higher at

288 some *cryaba* and *cryabb* mutant ages compared to wild-type larvae. Central disorganization of the lens

289 was only significantly increased in 4 dpf *cryaa* null larvae. Pitting was the most common defect seen in

290 wild-type larvae and not significantly increased in any of our mutant larvae.

291

292 All larvae used to assess lens phenotype were measured to record body length and lens diameter at 3

293 and 4 dpf (Fig. 5). These data show an increase in body length from 3 to 4 dpf in all genotypes, as

294 would be expected. Body length was more varied between two independent wild-type samples than

295 between wild-type and mutant samples, suggesting that gene knockout did not alter the overall fish

296 growth rate compared to wild-type fish. There appeared to be little to no difference in lens diameter

297 between the 3 and 4 dpf samples, which produced a decrease in the lens to body length ratio between

298 those two timepoints for all genotypes. The only measurement that was significantly different from

299 both wild-type samples was a reduced lens diameter of *cryabb* mutant larvae at 4 dpf.

300

301 *3.3. Loss of α-crystallins did not disrupt fiber cell denucleation*

302 Zebrafish lens fiber cells elongate and lose their nuclei between 2 and 3 dpf. We examined lenses

303 histologically at 3 and 4 dpf to determine if this process was altered by loss of each α-crystallin (Fig. 6).

304 Wild-type lenses showed that while the timing of this process can vary, the majority of lenses cleared

305 all nuclei from central fiber cells by 3 dpf, leaving elongated nuclei at the posterior margin (Fig. 6A,

306 white boxes). We consistently found two posterior zones of extended fiber cells bordering a

307 denucleated space between them (Fig. 6A, asterisk), with what appeared to be a single layer of nuclei

308 adjacent to the retinal neurons. Lenses contained rings of DAPI staining just anterior to the remaining,

309 elongated fiber cells and extending forward with a gap between the anterior margin and the epithelial

310 fiber cells (Fig. 6A, white arrows). The posterior-most gap between elongated fiber cells was a good

311 indicator that sections imaged were through the equator of the lens. Elongated fiber cell nuclei in wild-

312 type lenses ranged from flat to wavy and occasionally retained an oval shape (Fig. 6C, white arrow). At

313 4 dpf, the posterior fiber cell nuclei stacks appeared thinner, and DAPI rings were less common.

314

315 The lenses of *cryaa* null 3 dpf larvae also varied in their DAPI staining. However, more abnormal

316 phenotypes were seen. A small number of *cryaa* null lenses retained fiber cell nuclei deep to the

317 central DAPI staining ring (Fig. 6 I and J) or on the ring itself (Fig. 6H). Quantitation of pixel intensity

318 also showed that some *cryaa* null larval lenses had higher amounts of DAPI staining material in the

319 deeper parts of the cortex and lens nucleus, but the mean pixel intensity did not differ statistically from

320 that of wild-type larvae (Fig. 6N). None of the 4 dpf *cryaa* null larvae examined retained abnormal fiber

321 cell nuclei. None of the *cryaba* or *cryabb* mutant 3 dpf larvae examined showed retained fiber cell

322 nuclei within the central lens (Supplementary Fig. S2). However, some lenses did appear to have

8

323 thicker fiber cell nuclei stacks and possibly more nuclei with oval shape, although these features were
324 also seen in some wild-type lenses as described above.
325
326 *3.4. CRISPR deletion of each α-crystallin gene did not alter the expression of the other two*
327 Quantitative PCR (qPCR) was used to measure α-crystallin gene expression levels in wild-type and our
328 mutant lines. This allowed us to determine whether mutation led to a decrease in mRNA levels for the
329 damaged gene or changes in expression of the other α-crystallin genes. Whole larvae were assessed at
330 7 dpf, as earlier work showed low levels of *cryaba* and *cryabb* expression through 4 and 5 dpf,
331 respectively (Posner et al., 2017), and almost no expression in the lens (Farnsworth et al., 2021). We
332 found reduced levels of *cryaa* mRNA in 7 dpf homozygous *cryaa* mutants produced by deleting the
333 proximal promoter and start codon (Fig. 7A). The expression levels of *cryaa* did not change in *cryaba* or
334 *cryabb* mutant larvae compared to wild-type larvae (Fig. 7A). The *cryaba* and *cryabb* mutant lines were
335 not produced by deleting the promoter and start codon but instead were produced with a single gRNA
336 producing frame shift mutations and early stop codons (Fig. 3). *cryaba* mRNA levels were not different
337 in the *cryaba* mutant larvae compared to wild-type larvae, nor were they increased in the other
338 mutant lines (Fig. 7B). Messenger RNA for *cryabb* was reduced in *cryabb* mutant larvae compared to
339 other mutant lines (Fig. 7C). While the delta Cq values for *cryabb* mRNA in *cryabb* mutants were all
340 lower than those in wild-type larvae, this difference was not statistically significant. Messenger RNA
341 levels for *cryabb* were not significantly increased in *cryaa* or *cryaba* mutants compared to wild-type
342 larvae.
343
344
345 **4. Discussion**
346 We produced mutant zebrafish lines for each of the three α-crystallin proteins. Lack of αA-crystallin
347 caused a variety of visible lens defects in mutant larvae not seen or present at lower frequency in wild-
348 type larvae. Mutation of either αB-crystallin did not cause an increase in overall lens abnormalities,
349 although our *cryabb*-null line expressed a truncated αBb-crystallin. Loss of αA-crystallin did not alter
350 overall lens growth or significantly disrupt the fiber cell denucleation important for lens development.
351 Finally, none of the gene mutations produced compensatory changes in the mRNA levels of the others.
352 These data suggest that loss of αA-crystallin makes zebrafish lenses more susceptible to defects in
353 development but does not always trigger these defects. Loss of either αBa-crystallin or a full-length
354 αBb-crystallin produced little significant change in the lens through four days of development.
355
356 The observation of lens abnormalities in our CRISPR-produced *cryaa* null larvae agrees with previous
357 work done with a TALEN-produced *cryaa* knockout line (Zou et al., 2015). However, while lens images
358 from that study showed central roughness and pitting of the lens, the authors did not indicate the
359 central disorganization, peripheral fiber cell roughness or irregular fiber cell boundaries identified in
360 our *cryaa* null larvae. The proportion of null incross larvae with lens defects in the TALEN study was
361 approximately 85%, slightly more than our finding of 60%. That study separated their phenotypes into
362 "minor" and "major", with just over 40% of larvae having minor lens defects. Despite the different
363 methods used to characterize lens defects in our present study and this past TALEN work, it seems that
364 the observed penetrance of *cryaa* loss is comparable. It is notable that the effects of αA-crystallin loss
365 can range from no apparent defect in lens structure to a variety of defects that can occur singly or in

9

366 combination. A similar range of lens effects was seen after CRISPR knockout of the zebrafish aquaporin
367 0 paralogs, *mipa* and *mipb* (Vorontsova et al., 2018). Our results suggest that αA-crystallin is not
368 essential for proper lens development through 4 days post-fertilization but that its loss predisposes the
369 lens to defects. The only other model species with an αA-crystallin knockout line is the mouse (Brady
370 et al., 1997). Due to the *in utero* development of the mouse and its pigmentation, it was likely not
371 feasible to make similar observations of lens development at comparable stages to this study.
372 However, that study showed that *cryaa*-null mice develop cataracts by 7 weeks of age, indicating the
373 importance of the protein in lens biology. The impact of *cryaa* loss on zebrafish lens clarity as animals
374 age can be addressed in the future using our validated lines.
375
376 The impact of CRISPR-generated null mutation in *cryaa*, reported here, can be compared to prior
377 knockdowns by morpholino injection. We previously reported a lack of lens defects in zebrafish larval
378 lenses at 3 dpf after using a morpholino to block the translation of αA-crystallin (Posner et al., 2013).
379 Similar results were reported in a later study (Hinaux et al., 2014). Neither study imaged lenses using
380 DIC microscopy, so it is possible that defects such as those identified in the current study were missed.
381 It is also possible that small amounts of αA-crystallin produced during those morpholino experiments
382 were sufficient to prevent the defects found in this study.
383
384 Our data do not directly address the mechanisms behind the lens defects seen in our *cryaa* null lenses.
385 Histology and DAPI staining of 3 and 4 dpf larvae indicate that while there may be some delay in fiber
386 cell denucleation in *cryaa* null lenses, this delay was only found in a small proportion of lenses at 3 dpf
387 and gone by 4 dpf. Because αA-crystallin has documented functions as an anti-aggregation chaperone
388 that can buffer the effects of stress in the lens (Horwitz, 1992), it is possible that its loss may make the
389 lens more susceptible to protein aggregation. This likely led to the cataract seen in *cryaa* null mouse
390 lenses (Brady et al., 1997), and since zebrafish αA-crystallin has chaperone activity (Dahlman et al.,
391 2005; Koteiche et al., 2015), aggregates in central fiber cells may lead to observed central roughness.
392 This hypothesis could be tested by future proteomic analysis of insoluble proteins. Other defects we
393 observed hint at a breakdown in normal fiber cell arrangement. Under DIC imaging, the fiber cell
394 borders in the zebrafish lens were visible as regular concentric rings (Fig. 1D). Our observation of
395 central disorganization suggests defects in the arrangement of central fiber cells. A separate defect
396 appeared as short regions of rough, expanded space between peripheral fiber cells. These three
397 anatomical defects were visually distinct and may stem from different mechanistic defects in fiber cell
398 interactions. It has been proposed that αA-crystallin plays a direct role in fiber cell differentiation
399 (Boyle and Takemoto, 2000). While our *cryaa* null larvae did not show extended defects in fiber cell
400 nucleus degradation, there may be other aspects of fiber cell differentiation impacted by αA-crystallin
401 loss.
402
403 Our finding that lens diameters in *cryaa* null lenses at 3 and 4 dpf were similar to wild-type larvae
404 matches the results of a previous knockout study (Zou et al., 2015). Our *cryaba* and *cryabb* mutant
405 larvae also appeared similar in body length and lens diameter to wild-type larvae. We included two
406 separate samples of wild-type larvae to assess possible variation between breedings. The statistically
407 significant variation in body length between these two wild-type samples suggests that variation
408 between groups can be high and should be taken into account when looking for changes in lens growth

409 resulting from gene knockout. The observation that lens diameter was essentially unchanged between
410 3 and 4 dpf, while body length increased, was unexpected considering that past studies have found
411 linear relationships between lens diameter and body length, although these studies did not examine
412 fish prior to 7 dpf (Collery et al., 2014; Wang et al., 2020). It is possible that in these earlier stages,
413 body length and lens diameter growth are not parallel.

414

415 We found little evidence that mutation of either αB-crystallin gene in zebrafish caused abnormalities in
416 lens development or structure. Neither our *cryaba* nor *cryabb* mutant larvae showed a statistically
417 significant increase in the proportion of all lens defects compared to wild-type larvae (Fig. 4). Fiber cell
418 denucleation also appeared normal in both αB-crystallin mutant lines. The lack of developmental lens
419 defects in these fish is consistent with knockout studies in mice in which loss of the single αB-crystallin
420 gene had no effect on lens clarity through 39 weeks of age, although early developmental stages were
421 not examined (Brady et al., 2001). However, previously published CRISPR mutants for *cryaba* and
422 *cryabb* did produce lens defects at 4 dpf in a large proportion of larvae (Mishra et al., 2018). In that
423 study, approximately 75% and 50% of *cryaba*- and *cryabb*-null larvae, respectively, showed lens
424 abnormalities. Defects were categorized as "minor" and "major" with little description of defect type.
425 Two published images of lenses from a *cryaba* heterozygote cross show roughness or pitting as well as
426 some gaps between fiber cells. Previous work by the same lab identified far more severe lens defects in
427 zebrafish larvae after injection of translation-blocking morpholinos targeting *cryaba* and *cryabb* (Zou et
428 al., 2015). However, general gross defects in the resulting larvae suggest general toxicity from
429 morpholinos and not a lens-specific effect. In their more recent CRISPR lines, there were no reported
430 general larval defects, further suggesting that the morpholino-induced lens defects were not
431 specifically due to the loss of αB-crystallin proteins. While we found some significant increase in fiber
432 cell defects in our *cryaba* and *cryabb* mutant larvae compared to wild-type larvae, these proportions
433 were far lower than those reported in past studies.

434

435 Existing data suggest that neither *cryaba* nor *cryabb* are substantially expressed in the zebrafish lens
436 through 5 dpf based on shotgun proteomics (Greiling et al., 2009) and single-cell RNA-Seq (Farnsworth
437 et al., 2021). These published findings fit with the lack of significant early lens phenotypes in our αB-
438 crystallin mutant larvae. The reason for the discrepancy in our present CRISPR work and a past study
439 identifying lens defects in *cryaba* and *cryabb* knockout zebrafish (Mishra et al., 2018) is unclear. Our
440 mass spectrometry data indicated a total loss of all detectable αBa-crystallin peptides in *cryaba* null
441 adult lenses, indicating that our *cryaba* null line is incapable of producing αBa-crystallin protein.
442 However, the presence of the αBb-crystallin peptide 82-92 in adult lenses from our *cryabb* null line
443 suggest that these fish are capable of producing a truncated protein likely spanning residues 59-165.
444 This truncated C-terminal αBb-crystallin would contain the anti-aggregation chaperone site identified
445 in mammalian αB-crystallin (Bhattacharyya et al., 2006). Since this αBb-crystallin peptide was
446 identified by analyzing adult lenses our data do not indicate that this partial αBb-crystallin protein is
447 produced in larval lenses at the ages analyzed in this study (3 and 4 dpf). The production of a partial
448 protein even after a frame-shift mutation highlights the value in using mass spectrometry to confirm
449 the total loss of expression from a CRISPR targeted gene.

450

451   The variety of approaches used to produce αA-crystallin mutants in this study allows us to compare
452   their utility for studying resulting phenotypes. The quickest way to screen genes for their role in
453   development is to directly examine larvae injected at the zygote state (crispants). There is good
454   evidence that this approach is effective when injecting a mix of four gRNAs (Wu et al., 2018). In our
455   own hands, we found this approach effective when targeting genes already known to play an essential
456   role in lens development. For example, injection of a four-gRNA mix targeting the transcription factor
457   *foxe3* closely replicated phenotypes reported in a stable zebrafish null line (Supplementary Fig. S3;
458   (Krall and Lachke, 2018)). However, when targeting *cryaa,* this approach did not produce similar levels
459   of phenotypes seen in our null line (Fig. 4). The proportion of each defect differed between the two
460   approaches, and the levels of some defects also differed between 3 and 4 dpf. These variations in
461   phenotype could be due to the mosaic nature of gRNA-injected larvae, in which some lens cells contain
462   mutant *cryaa* alleles and others contain wild-type alleles. The expression of αA-crystallin in unaffected
463   cells may be enough to prevent the defects seen in our null line. We previously showed that adult
464   zebrafish lenses produce less αA-crystallin than mammalian lenses (Posner et al., 2008), and our past
465   qPCR and single-cell RNA-Seq data suggest that lens *cryaa* expression through 5 dpf is relatively low as
466   well (Farnsworth et al., 2021; Posner et al., 2017). Since the complete loss of αA-crystallin in our *cryaa*
467   null line only led to visible defects in 60% of larvae, the expression of reduced amounts in our injected
468   embryos may be sufficient to suppress the phenotype. It is also possible that differences are simply
469   due to the stochastic nature of phenotype development. Considering the dynamic changes occurring in
470   the zebrafish lens between 3 and 4 dpf, it is best to quantify phenotypes for each day separately in
471   future studies.

473   Because our initial *cryaa* null line generated with a single gRNA and containing a frameshift mutation
474   stopped breeding, we took the opportunity to generate a second null line with a large deletion
475   removing the proximal promoter region and start codon. Both lines generated similar lens defects,
476   reinforcing the conclusion that these defects resulted from the loss of αA-crystallin and not off-target
477   effects. There are two other benefits to generating mutant knockout alleles by deletion. First, these
478   deletion alleles are simpler to screen, as they are identifiable by PCR without subsequent sequencing.
479   Second, deletion of the promoter and start codon reduces the chance of possible genetic
480   compensation after nonsense-mediated mRNA decay (El-Brolosy et al., 2019). The loss of the targeted
481   gene's mRNA can also be monitored by qPCR (Fig. 7). Our two αB-crystallin mutant lines were
482   produced with single gRNAs and frameshift mutations. While our proteomics work analyzed the loss of
483   each protein in our null adult fish lenses, qPCR showed a reduction in *cryabb* mRNA in the *cryabb* null
484   line but no reduction in *cryaba* mRNA in the *cryaba* null line. This difference may reflect the
485   unpredictability of nonsense-mediated decay and shows that mRNA levels do not necessarily reflect
486   eventual protein levels. It is also possible that this difference in mRNA levels reflects primer location, as
487   our *cryaba* qPCR primers annealed within exon 1, just downstream of the gRNA target site, while our
488   *cryabb* primers annealed to the 5' UTR.

490   Several key questions remain unanswered in this study. It is unclear how the loss of αA-crystallin leads
491   to the visual defects observed by DIC microscopy. Lenses from mutant α-crystallin mice have been
492   analyzed by proteomics and RNA-Seq to identify changes in global gene expression (Andley et al., 2018,
493   2013). A similar approach would be valuable with our zebrafish null lines. We have only presented data

494   through 7 dpf. It will be interesting to see how αA-crystallin loss impacts lens clarity and optics as fish
495   age. While we know that both αB-crystallin genes are expressed in the adult lens, we do not know at
496   what age this expression begins and how αB-crystallin loss may impact lenses as they age. This
497   question is particularly interesting, as *cryaba* is lens specific in adults, while *cryabb* is expressed
498   broadly, suggesting an ontogenetic shift in the function of these genes and their proteins. Why *cryaba*
499   is expressed outside the lens in early development and whether it or *cryabb* plays an important
500   developmental role in those extralenticular tissues are also unknown. Answers to these questions
501   would add to the understanding of why these small heat shock protein genes were coopted as key
502   players during vertebrate lens evolution.

503

504

Acknowledgments

514

Author Contributions

516   MP conceived and designed the study. KZ and LLD designed and conducted the proteomic
517   experiments. MP, KLM, BA, SB, AR, KF, AH, TK, EK, MSM and TS contributed to the production of
518   CRISPR null lines and/or analyzed the resulting phenotypes. MP, KLM, AR, AH, TK, and LLD wrote the
519   manuscript. All authors reviewed the manuscript.

520

Data Availability

522   Data spreadsheets and R scripts used for Figures 4-7 can be found in the following GitHub repository:
523   github.com/masonfromohio/alpha-crystallin-CRISPR-Rscripts. DIC images and DAPI images of lenses
524   will be made available on Dryad.org. Skyline analysis of mass spectrometry data will be made available
525   on PanoramaWeb (panoramaweb.org)

526

527

528

529

References

Andley, U.P., Malone, J.P., Hamilton, P.D., Ravi, N., Townsend, R.R., 2013. Comparative Proteomic Analysis Identifies Age-Dependent Increases in the Abundance of Specific Proteins after Deletion of the Small Heat Shock Proteins αA- and αB-Crystallin. Biochemistry-us 52, 2933–2948. https://doi.org/10.1021/bi400180d

Andley, U.P., Tycksen, E., McGlasson-Naumann, B.N., Hamilton, P.D., 2018. Probing the changes in gene expression due to α-crystallin mutations in mouse models of hereditary human cataract. PLoS ONE 13, e0190817-18. https://doi.org/10.1371/journal.pone.0190817

Bhattacharyya, J., Udupa, E.G.P., Wang, J., Sharma, K.K., 2006. Mini-αB-Crystallin: A Functional Element of αB-Crystallin with Chaperone-like Activity †. Biochemistry 45, 3069–3076. https://doi.org/10.1021/bi0518141

Bova, M.P., Yaron, O., Huang, Q., Ding, L.L., Haley, D.A., Stewart, P.L., Horwitz, J., 1999. Mutation R120G in alphaB-crystallin, which is linked to a desmin-related myopathy, results in an irregular structure and defective chaperone-like function. Proceedings of the National Academy of Sciences of the United States of America 96, 6137–6142.

Boyle, D.L., Takemoto, L.J., 2000. A possible role for alpha-crystallins in lens epithelial cell differentiation. Molecular vision 6, 63–71.

Brady, J.P., Garland, D., Duglas-Tabor, Y., Robison, W.G., Groome, A., Wawrousek, E.F., 1997. Targeted disruption of the mouse alpha A-crystallin gene induces cataract and cytoplasmic inclusion bodies containing the small heat shock protein alpha B-crystallin. Proceedings of the National Academy of Sciences of the United States of America 94, 884–889.

Brady, J.P., Garland, D.L., Green, D.E., Tamm, E.R., Giblin, F.J., Wawrousek, E.F., 2001. AlphaB-crystallin in lens development and muscle integrity: a gene knockout approach. Investigative ophthalmology & visual science 42, 2924–2934.

Bustin, S.A., Benes, V., Garson, J.A., Hellemans, J., Huggett, J., Kubista, M., Mueller, R., Nolan, T., Pfaffl, M.W., Shipley, G.L., Vandesompele, J., Wittwer, C.T., 2009. The MIQE guidelines: minimum information for publication of quantitative real-time PCR experiments.

Collery, R.F., Veth, K.N., Dubis, A.M., Carroll, J., Link, B.A., 2014. Rapid, Accurate, and Non-Invasive Measurement of Zebrafish Axial Length and Other Eye Dimensions Using SD-OCT Allows Longitudinal Analysis of Myopia and Emmetropization. Plos One 9, e110699. https://doi.org/10.1371/journal.pone.0110699

14

563 Dahlman, J.M., Margot, K.L., Ding, L., Horwitz, J., Posner, M., 2005. Zebrafish alpha-crystallins: protein
564   structure and chaperone-like activity compared to their mammalian orthologs. Molecular vision 11,
565   88–96.

566 El-Brolosy, M.A., Kontarakis, Z., Rossi, A., Kuenne, C., Günther, S., Fukuda, N., Kikhi, K., Boezio, G.L.M.,
567   Takacs, C.M., Lai, S.-L., Fukuda, R., Gerri, C., Giraldez, A.J., Stainier, D.Y.R., 2019. Genetic
568   compensation triggered by mutant mRNA degradation. Nature 1–26.
569   https://doi.org/10.1038/s41586-019-1064-z

570 Farnsworth, D., Posner, M., Miller, A., 2021. Single cell transcriptomics of the developing zebrafish lens
571   and identification of putative controllers of lens development. Exp Eye Res 108535.
572   https://doi.org/10.1016/j.exer.2021.108535

573 Greiling, T.M.S., Aose, M., Clark, J.I., 2010. Cell fate and differentiation of the developing ocular lens.
574   Investigative ophthalmology & visual science 51, 1540–1546. https://doi.org/10.1167/iovs.09-4388

575 Greiling, T.M.S., Houck, S.A., Clark, J.I., 2009. The zebrafish lens proteome during development and
576   aging. Molecular vision 15, 2313–2325.

577 Hinaux, H., Blin, M., Fumey, J., Legendre, L., Heuzé, A., Casane, D., Rétaux, S., 2014. Lens defects in
578   Astyanax mexicanusCavefish: Evolution of crystallins and a role for alphaA-crystallin. Developmental
579   neurobiology n/a-n/a. https://doi.org/10.1002/dneu.22239

580 Horwitz, J., 1992. Alpha-crystallin can function as a molecular chaperone. Proceedings of the National
581   Academy of Sciences of the United States of America 89, 10449–10453.

582 Kilkenny, C., Browne, W.J., Cuthill, I.C., Emerson, M., Altman, D.G., 2010. Improving Bioscience
583   Research Reporting: The ARRIVE Guidelines for Reporting Animal Research. Plos Biol 8, e1000412.
584   https://doi.org/10.1371/journal.pbio.1000412

585 Koteiche, H.A., Claxton, D.P., Mishra, S., Stein, R.A., McDonald, E.T., McHaourab, H.S., 2015. Species-
586   Specific Structural and Functional Divergence of α-Crystallins: Zebrafish αBa- and Rodent αA ins-
587   Crystallin Encode Activated Chaperones. Biochemistry 54, 5949–5958.
588   https://doi.org/10.1021/acs.biochem.5b00678

589 Krall, M., Lachke, S.A., 2018. A zebrafish model of foxe3 deficiency demonstrates lens and eye defects
590   with dysregulation of key genes involved in cataract formation in humans. Human genetics 137,
591   315–328. https://doi.org/10.1007/s00439-018-1884-1

592 Mishra, S., Wu, S.-Y., Fuller, A.W., Wang, Z., Rose, K.L., Schey, K.L., McHaourab, H.S., 2018. Loss of αB-
593   crystallin function in zebrafish reveals critical roles in the development of the lens and stress
594   resistance of the heart. The Journal of biological chemistry 293, 740–753.
595   https://doi.org/10.1074/jbc.m117.808634

596 Pino, L.K., Searle, B.C., Bollinger, J.G., Nunn, B., MacLean, B., MacCoss, M.J., 2020. The Skyline
597   ecosystem: Informatics for quantitative mass spectrometry proteomics. Mass Spectrom Rev 39,
598   229–244. https://doi.org/10.1002/mas.21540

599 Posner, M., Hawke, M., Lacava, C., Prince, C.J., Bellanco, N.R., Corbin, R.W., 2008. A proteome map of
600   the zebrafish (Danio rerio) lens reveals similarities between zebrafish and mammalian crystallin
601   expression. Molecular vision 14, 806–814.

602 Posner, M., Murray, K.L., McDonald, M.S., Eighinger, H., Andrew, B., Drossman, A., Haley, Z.,
603   Nussbaum, J., David, L.L., Lampi, K.J., 2017. The zebrafish as a model system for analyzing
604   mammalian and native α-crystallin promoter function. PeerJ 5, e4093-27.
605   https://doi.org/10.7717/peerj.4093

606 Posner, M., Skiba, J., Brown, M., Liang, J.O., Nussbaum, J., Prior, H., 2013. Loss of the small heat shock
607   protein αA-crystallin does not lead to detectable defects in early zebrafish lens development.
608   Experimental Eye Research. https://doi.org/10.1016/j.exer.2013.09.007

609 Smith, A.A., Wyatt, K., Vacha, J., Vihtelic, T.S., Zigler, J.S., Wistow, G.J., Posner, M., 2006. Gene
610   duplication and separation of functions in alphaB-crystallin from zebrafish (Danio rerio). The FEBS
611   journal 273, 481–490. https://doi.org/10.1111/j.1742-4658.2005.05080.x

612 Srinivasan, A.N., Nagineni, C.N., Bhat, S.P., 1992. alpha A-crystallin is expressed in non-ocular tissues.
613   The Journal of biological chemistry 267, 23337–23341.

614 Team, R.C., 2020. R: A language and environment for statistical computing [WWW Document]. URL
615   https://www.R-project.org/

616 Team, Rs., 2020. RStudio: Integrated Development Environment for R [WWW Document]. URL
617   http://www.rstudio.com/

618 Vorontsova, I., Gehring, I., Hall, J.E., Schilling, T.F., 2018. Aqp0a Regulates Suture Stability in the
619   Zebrafish Lens. Investigative ophthalmology & visual science 59, 2869–11.
620   https://doi.org/10.1167/iovs.18-24044

621 Wang, K., Vorontsova, I., Hoshino, M., Uesugi, K., Yagi, N., Hall, J.E., Schilling, T.F., Pierscionek, B.K.,
622   2020. Optical development in the zebrafish eye lens. FASEB journal : official publication of the
623   Federation of American Societies for Experimental Biology 95, 399–11.
624   https://doi.org/10.1096/fj.201902607r

625 Wu, R.S., Lam, I.I., Clay, H., Duong, D.N., Deo, R.C., Coughlin, S.R., 2018. A Rapid Method for Directed
626   Gene Knockout for Screening in G0 Zebrafish. Developmental Cell 46, 112-125.e4.
627   https://doi.org/10.1016/j.devcel.2018.06.003

628   Zou, P., Wu, S.-Y., Koteiche, H.A., Mishra, S., Levic, D.S., Knapik, E., Chen, W., McHaourab, H.S., 2015. A
629   conserved role of αA-crystallin in the development of the zebrafish embryonic lens. Experimental
630   Eye Research 138, 104–113. https://doi.org/10.1016/j.exer.2015.07.001

631

632

633   **Figure Legends**

634

635   **Figure 1. *cryaa* null mutant.** Produced with a single gRNA to generate a five basepair deletion and
636   frame shift mutation in exon 1, with the relative position noted by the red line (A). Injected embryos
637   were outcrossed to wild-type fish to identify heterozygote mutants, with a five-base pair deletion allele
638   identified that leads to an early stop codon after amino acid 28 (B). Incrossed heterozygotes were used
639   to generate a homozygous null line, which was bred to assess the effects of *cryaa* loss. Mass
640   spectrometry confirmed that embryos generated by incrossing this null line produced no detectable
641   αA crystallin protein (C). Parallel reaction monitoring of the 3 major fragment ions of the +3 charge
642   state of *cryaa* peptide 52-65 from the digest of wild-type lenses showed coelution of its three major
643   fragment ions on the left and no corresponding peaks in the digest from KO lenses on the right (C).
644   Compared to wild-type lenses at 3 dpf (C), *cryaa* null embryos showed various defects, such as
645   roughness in the primary fiber cell region (E) and a general disorganization of central fiber cells (F).
646   Lenses are from 3 dpf embryos, imaged using DIC optics and arranged with retina to the left. Scale bars
647   are 20 microns.

648

649   **Figure 2. The second *cryaa* null mutant line generated by deleting the start codon and proximal
650   promoter region produced variable lens phenotypes.** Two gRNAs were designed to remove
651   approximately 860 base pairs of the *cryaa* gene (A). This large deletion could be easily identified using
652   PCR amplification with primers flanking the gRNA target regions (B). Some *cryaa* null embryos showed
653   visually normal lenses by DIC imaging (C, compare to wild type lens in Fig. 1D). Typical phenotypes in
654   abnormal lenses included roughness in central primary fiber cells (d) and general disorganization of
655   central fiber cells (e), as seen in our single gRNA null mutant (Fig. 1). Gaps or roughness between
656   peripheral fiber cells were also common (D and E: arrows). Some lenses combined several of these
657   phenotypes (F). We also observed lenses with severe boundaries between fiber cells (G: arrows) and
658   pitting (H). Lenses shown are either 3 or 4 dpf and arranged with retina to the left. Scale bars are 20
659   microns. Matching embryos for lenses E and F are shown to indicate a lack of general morphological
660   defects (E' and F').

661

662   **Figure 3. Production of *cryaba* and *cryabb* frameshift mutants.** Single gRNAs were designed to target
663   the first exons of the zebrafish *cryaba* (A) and *cryabb* (D) genes. After injection into wild-type zygotes,
664   founders were outcrossed to wild-type fish, and resulting heterozygotes with deletions that caused
665   frameshift mutations leading to early stop codons were detected (B and E). Mass spectrometry analysis
666   of adult lenses from mutant lines confirmed the loss of protein coded by each gene. Parallel reaction
667   monitoring of the +3 charge state of αBa-crystallin tryptic peptide 80-89 from the digest of wild-type
668   lenses detected coelution of its three major fragment ions (left), and these were not detectable in
669   *cryaba* mutant adult lenses (C). Similarly, the +2 charge state of αBb-crystallin tryptic peptide 12-20

670 from the digest of wild-type lenses detected coelution of its three major fragment ions (left), and these
671 were missing in digests from *cryabb* mutant adult lenses on the right (F).

672 **Figure 4. Prevalence of different lens abnormalities in wild-type, α-crystallin mutant and *cryaa***
673 **gRNA-injected larvae at 3 and 4 dpf.** Each graph shows the proportion of larvae with that defect type.
674 Larvae examined at 3 and 4 dpf were wild-type (n= 36/38), offspring of homozygous mutants for *cryaa*
675 (n=41/35), *cryaba* (n=40/34) and *cryabb* (n=38/28), and embryos injected with a four-gRNA mix
676 targeting the *cryaa* gene (crispants; n=27/16). Asterisks indicate statistically significant differences
677 from age-matched wild-type larvae ("N-1" Chi-squared test).

678 **Figure 5. Comparison of lens diameters and body lengths between wild-type and α-crystallin**
679 **knockout embryos.** Box and whisker plots show measurements at 3 and 4 days post-fertilization (dpf).
680 Analysis of variance with Tukey's post-test was used to identify statistically significant differences
681 between groups. Letters indicate statistical groups within each panel.

682 **Figure 6. Cryosectioned lenses at 3 and 4 dpf were stained with DAPI to assess the clearance of fiber**
683 **cell nuclei.** Four representative lenses are shown for the wild-type (A-D) and *cryaa* null lines (G-J) at 3
684 dpf, and two representative lenses are shown at 4 dpf (E-F; K-L). Most images were taken at 200X total
685 magnification, with some taken at 100X to capture more lens cell nuclei in one focal plane. The retina is
686 oriented to the left in each image, with the cornea to the right. The four images at 3 dpf for each
687 genotype demonstrate the range of phenotypes found, with the top left panel the most normal and
688 bottom right the most abnormal. The rectangle in panel A highlights one of two regions of flattened,
689 extended fiber cell nuclei at the retinal side of the lens, separated by a nucleus-free zone at *. Arrows
690 indicate details described in the results section. Concentric circles were used to measure the average
691 pixel density of DAPI staining across the lens (see M as an example). While some *cryaa* null lenses
692 showed higher DAPI intensity in inner areas of the lens at 3 dpf (N), these differences were not
693 statistically significant (Mann–Whitney U test).

694 **Figure 7. Expression of each α-crystallin gene assayed by qPCR in whole bodies of wild-type and**
695 **mutant larvae at 7 dpf.** Box and whisker plots show delta Cq values generated with primers for *cryaa*
696 (A), *cryaba* (B) and *cryabb* (C) in three biological replicates of the genotypes indicated on the x-axes. Y-
697 axes are inverted, as lower delta Cq values indicate greater expression. Asterisks indicate statistically
698 significant differences based on ANOVA with Tukey's post-hoc test (*p value* < 0.05).
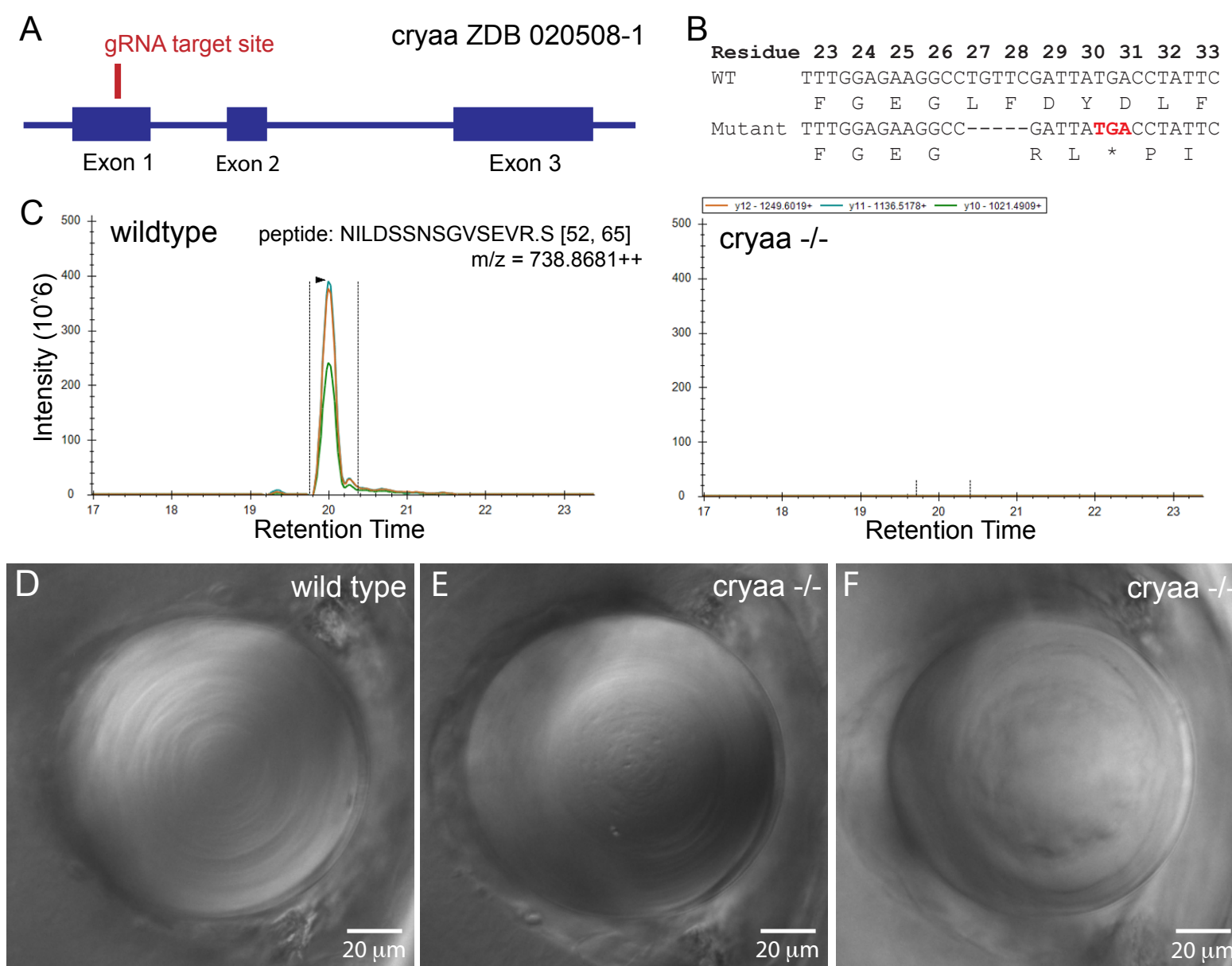
18

Figure 1

Figure 1. *cryaa* null mutant. Produced with a single gRNA to generate a five basepair deletion and frame shift mutation in exon 1, with the relative position noted by the red line (A). Injected embryos were outcrossed to wild-type fish to identify heterozygote mutants, with a five-base pair deletion allele identified that leads to an early stop codon after amino acid 28 (B). Incrossed heterozygotes were used to generate a homozygous null line, which was bred to assess the effects of *cryaa* loss. Mass spectrometry confirmed that embryos generated by incrossing this null line produced no detectable αA crystallin protein (C). Parallel reaction monitoring of the 3 major fragment ions of the +3 charge state of *cryaa* peptide 52-65 from the digest of wild-type lenses showed coelution of its three major fragment ions on the left and no corresponding peaks in the digest from KO lenses on the right (C). Compared to wild-type lenses at 3 dpf (D), *cryaa* null embryos showed various defects, such as roughness in the primary fiber cell region (E) and a general disorganization of central fiber cells (F). Lenses are from 3 dpf embryos, imaged using DIC optics and arranged with retina to the left. Scale bars are 20 microns.

Figure 2
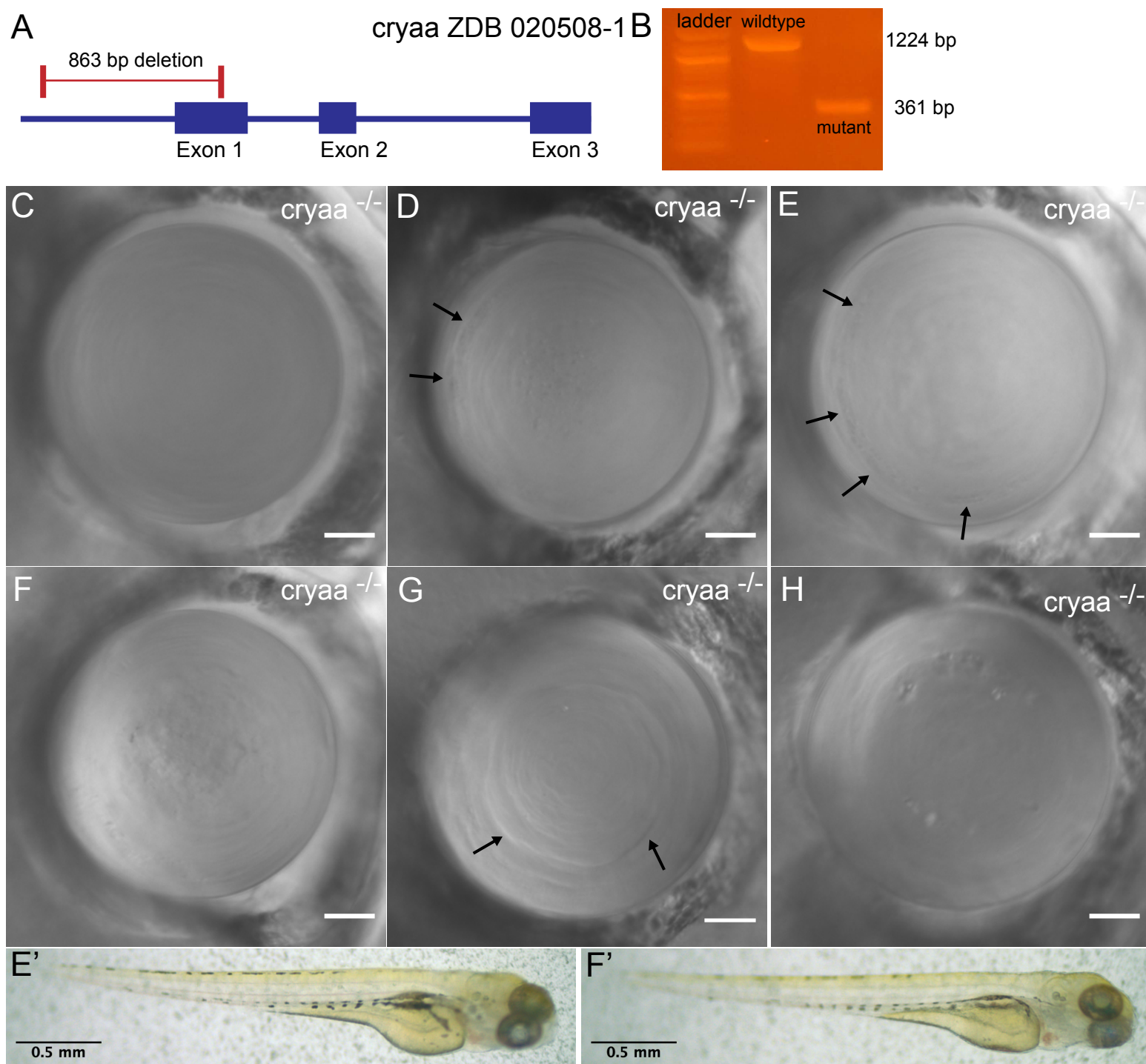
Figure 2. The second *cryaa* null mutant line generated by deleting the start codon and proximal promoter region produced variable lens phenotypes. Two gRNAs were designed to remove approximately 860 base pairs of the cryaa gene (A). This large deletion could be easily identified using PCR amplification with primers flanking the gRNA target regions (B). Some *cryaa* null embryos showed visually normal lenses by DIC imaging (C, compare to wild type lens in Fig. 1D). Typical phenotypes in abnormal lenses included roughness in central primary fiber cells (D) and general disorganization of central fiber cells (E), as seen in our single gRNA null mutant (Fig. 1). Gaps or roughness between peripheral fiber cells were also common (D and E: arrows). Some lenses combined several of these phenotypes (F). We also observed lenses with severe boundaries between fiber cells (G: arrows) and pitting (H). Lenses shown are either 3 or 4 dpf and arranged with retina to the left. Scale bars are 20 microns. Matching embryos for lenses E and F are shown to indicate a lack of general morphological defects (E' and F').

Figure 3
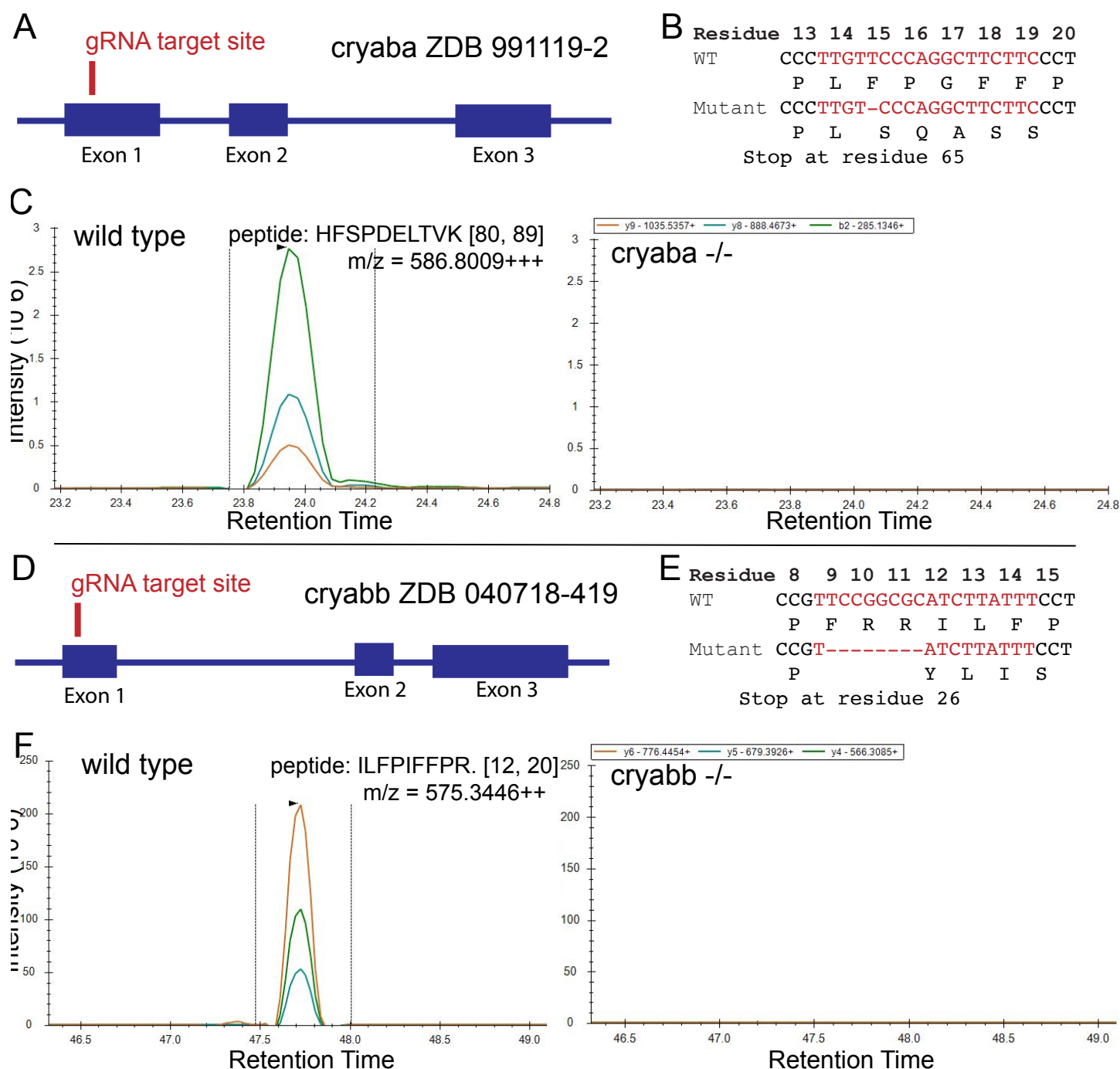
Figure 3. Production of *cryaba* and *cryabb* frameshift mutants. Single gRNAs were designed to target the first exons of the zebrafish *cryaba* (A) and *cryabb* (D) genes. After injection into wild-type zygotes, founders were outcrossed to wild-type fish, and resulting heterozygotes with deletions that caused frameshift mutations leading to early stop codons were detected (B and E). Mass spectrometry analysis of adult lenses from mutant lines confirmed the loss of protein coded by each gene. Parallel reaction monitoring of the +3 charge state of αBa-crystallin tryptic peptide 80-89 from the digest of wild-type lenses detected coelution of its three major fragment ions (left), and these were not detectable in *cryaba* mutant adult lenses (C). Similarly, the +2 charge state of αBb-crystallin tryptic peptide 12-20 from the digest of wild-type lenses detected coelution of its three major fragment ions (left), and these were missing in digests from *cryabb* mutant adult lenses on the right (F).

Figure 4
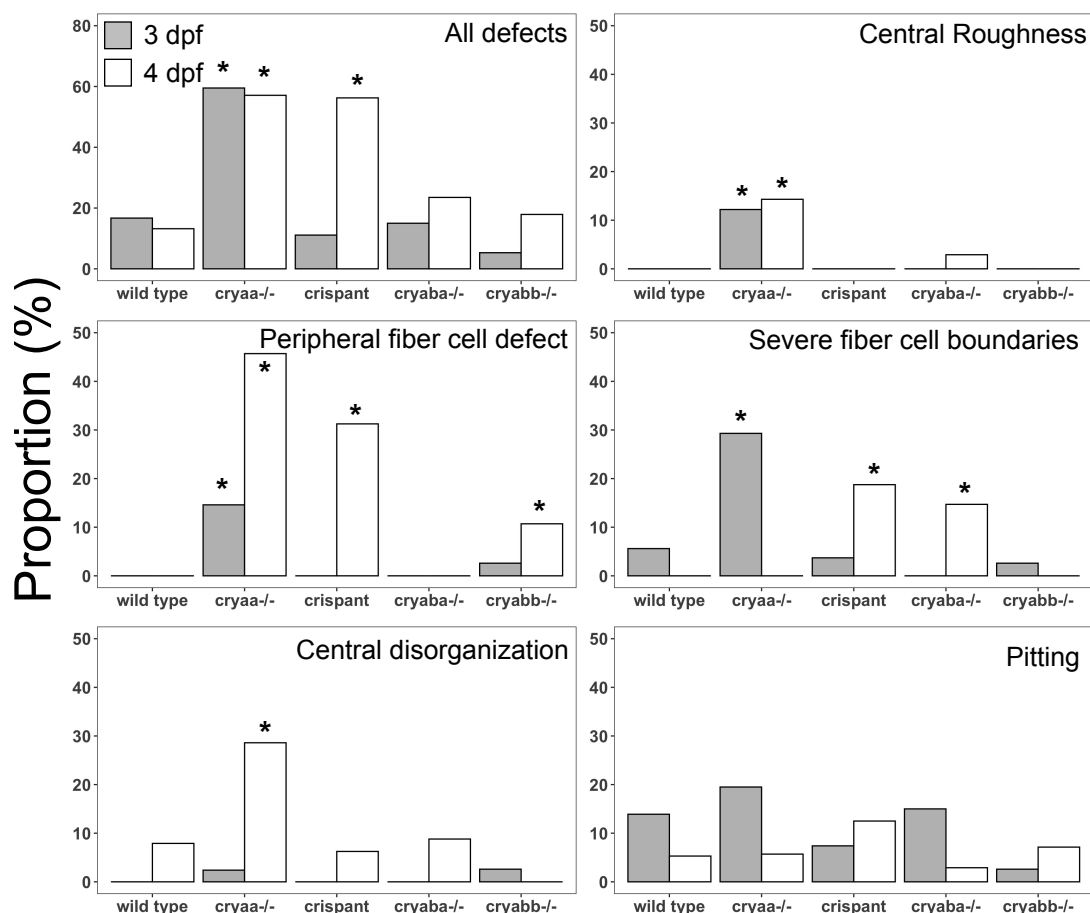
Figure 4. Prevalence of different lens abnormalities in wild-type, α-crystallin mutant and *cryaa* gRNA-injected larvae at 3 and 4 dpf. Each graph shows the proportion of larvae with that defect type. Larvae examined at 3 and 4 dpf were wild-type (n= 36/38), offspring of homozygous mutants for *cryaa* (n=41/35), *cryaba* (n=40/34) and *cryabb* (n=38/28), and embryos injected with a four-gRNA mix targeting the *cryaa* gene (crispants; n=27/16). Asterisks indicate statistically significant differences from age-matched wild-type larvae ("N-1" Chi-squared test).

Figure 5
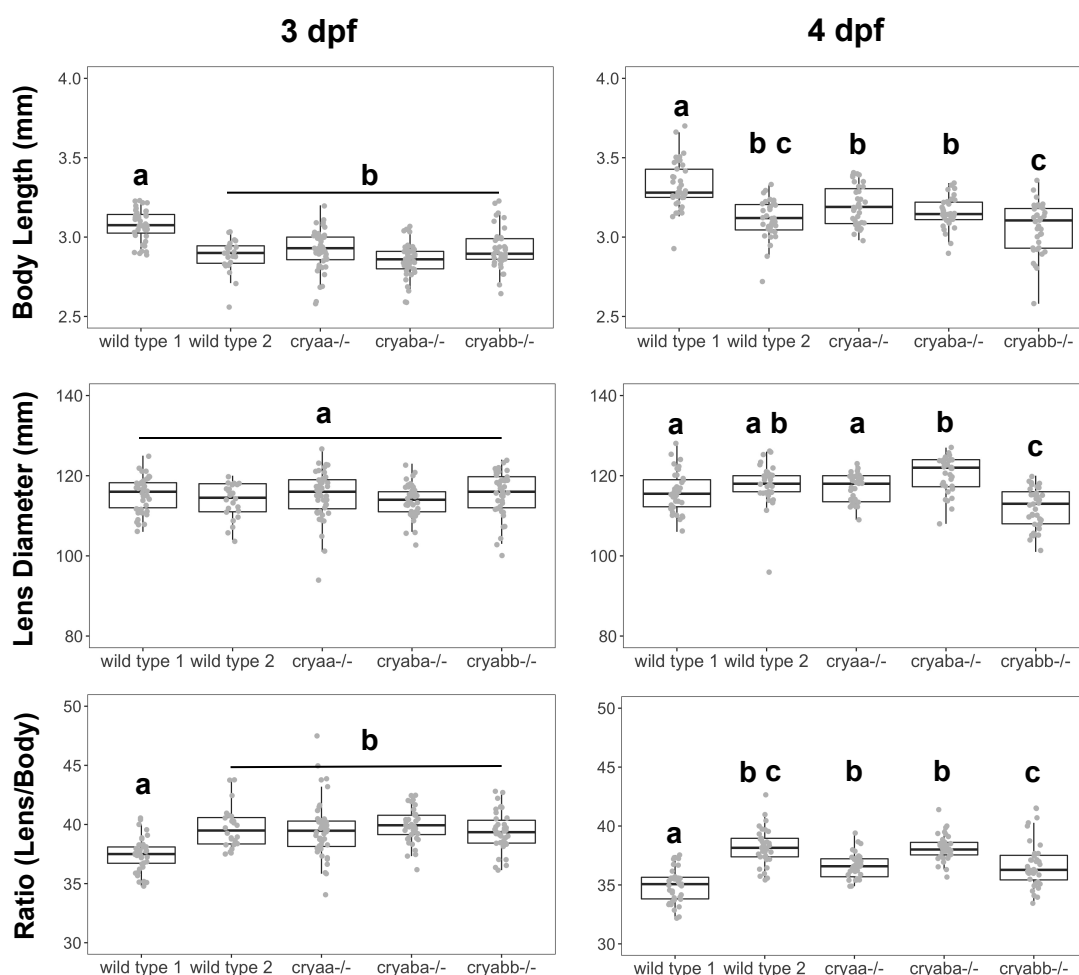
Figure 5. Comparison of lens diameters and body lengths between wild-type and α-crystallin knockout embryos. Box and whisker plots show measurements at 3 and 4 days post-fertilization (dpf). Analysis of variance with Tukey's post-test was used to identify statistically significant differences between groups. Letters indicate statistical groups within each panel.
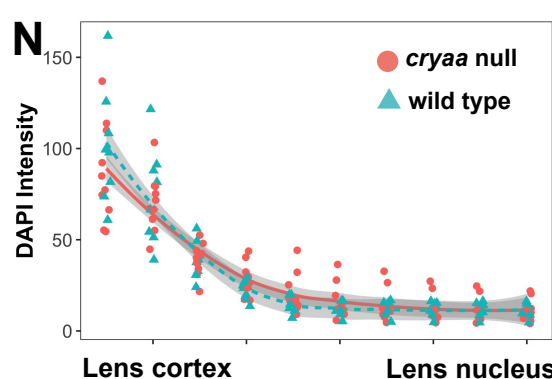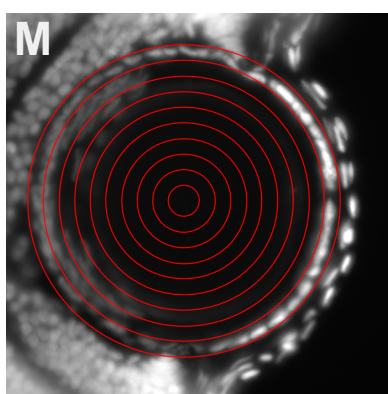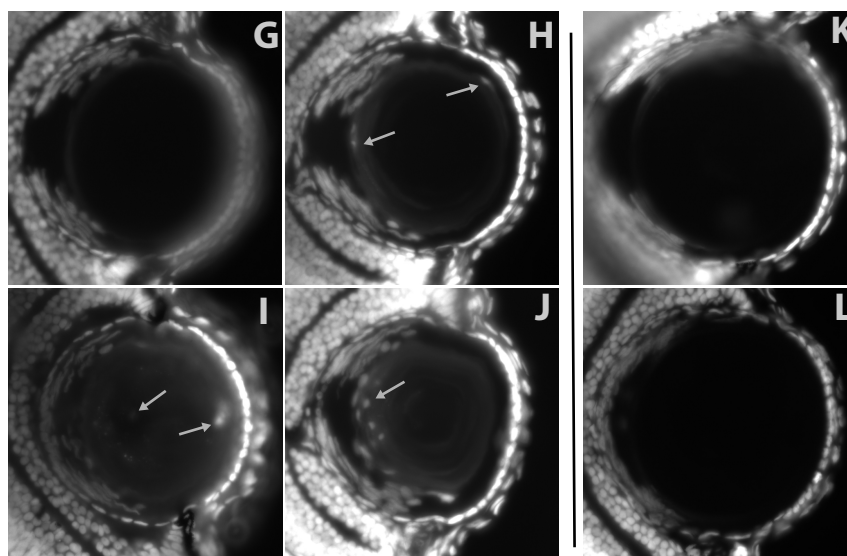
Figure 6
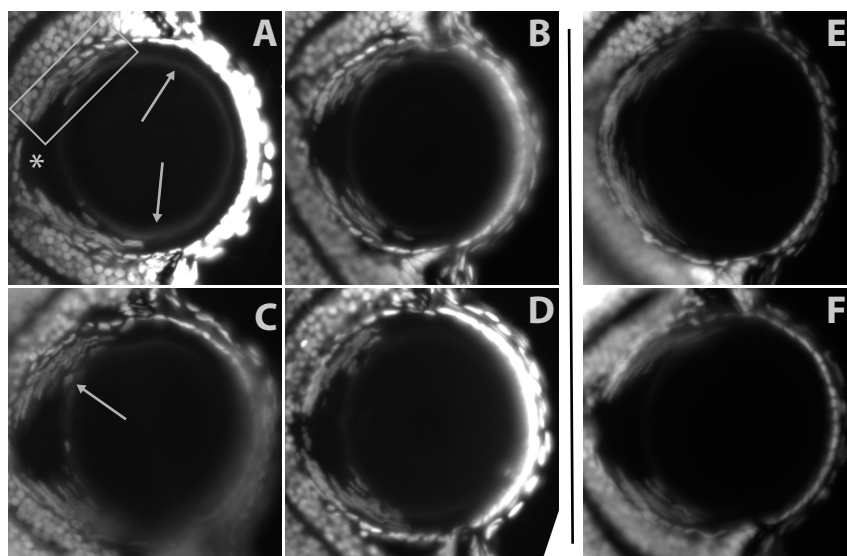
Figure 6. Cryosectioned lenses at 3 and 4 dpf were stained with DAPI to assess the clearance of fiber cell nuclei. Four representative lenses are shown for the wild-type (A-D) and *cryaa* null lines (G-J) at 3 dpf, and two representative lenses are shown at 4 dpf (E-F; K-L). Most images were taken at 200X total magnification, with some taken at 100X to capture more lens cell nuclei in one focal plane. The retina is oriented to the left in each image, with the cornea to the right. The four images at 3 dpf for each genotype demonstrate the range of phenotypes found, with the top left panel the most normal and bottom right the most abnormal. The rectangle in panel A highlights one of two regions of flattened, extended fiber cell nuclei at the retinal side of the lens, separated by a nucleus-free zone at *. Arrows indicate details described in the results section. Concentric circles were used to measure the average pixel density of DAPI staining across the lens (see M as an example). While some *cryaa* null lenses showed higher DAPI intensity in inner areas of the lens at 3 dpf (N), these differences were not statistically significant (Mann–Whitney U test).
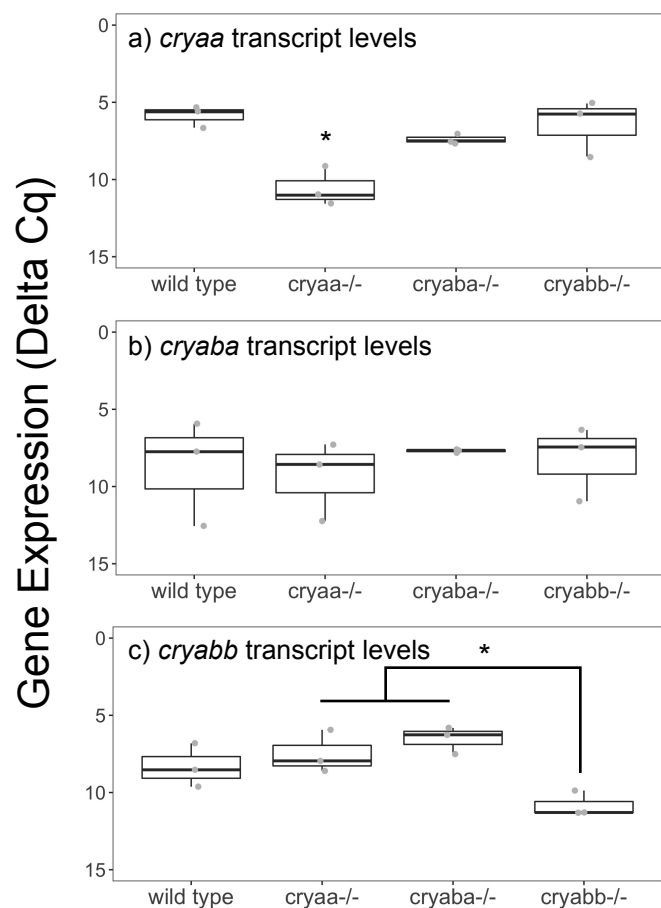
Figure 7

Figure 7. Expression of each α-crystallin gene assayed by qPCR in whole bodies of wild-type and mutant larvae at 7 dpf. Box and whisker plots show delta Cq values generated with primers for *cryaa* (a), *cryaba* (b) and *cryabb* (c) in three biological replicates of the genotypes indicated on the x-axes. Y-axes are inverted, as lower delta Cq values indicate greater expression. Asterisks indicate statistically significant differences based on ANOVA with Tukey's post-hoc test (*p value* < 0.05).